Journal of Power Sources 421 (2019) 91–99

Contents lists available at ScienceDirect

Journal of Power Sources

journal homepage: www.elsevier.com/locate/jpowsour

Mixed-conducting interlayer boosting the electrochemical performance of Ni-rich layered oxide cathode materials for lithium ion batteries

Qinglu Fan[a,b], Shaodian Yang[a,b], Jun Liu[a,b], Haodong Liu[c], Kaiji Lin[a,b], Rui Liu[d], Chaoyu Hong[d], Liying Liu[a,b], Yan Chen[e], Ke An[e], Ping Liu[c], Zhicong Shi[a,b,*], Yong Yang[d,**]

[a] *School of Materials and Energy, Guangdong University of Technology, Guangzhou, 510006, PR China*
[b] *Guangdong Engineering Technology Research Center for New Energy Materials and Devices, Guangzhou, 510006, PR China*
[c] *Department of Nanoengineering, University of California San Diego, CA, 92093, USA*
[d] *Department of Chemistry, Xiamen University, Xiamen, 361005, PR China*
[e] *Neutron Scattering Division, Oak Ridge National Laboratory, Oak Ridge, TN, 37830, USA*

HIGHLIGHTS

- The residual Li species on the surface of NCM811 were transformed into Li_3PO_4.
- Build a mixed-conducting interlayer with fast ionic and electronic conductivities.
- The modified samples show excellent cycling stability and high rate performance.
- The performance of NCM811 was enhanced at both room and high temperature.
- The mixed-conducting interlayer improves the thermal stability of NCM811.

ARTICLE INFO

Keywords:
$LiNi_{0.8}Co_{0.1}Mn_{0.1}O_2$
Li_3PO_4
Graphene
Mixed-conducting interlayer
Synergistic effect

ABSTRACT

In this work, a unique artificial interface combing characteristics of both high ionic and electronic conductivities has been successfully constructed at the surface of Ni-rich $LiNi_{0.8}Co_{0.1}Mn_{0.1}O_2$ (NCM811). The ionic conductor layer is fabricated through reacting H_3PO_4 with the lithium residuals on the surface of NCM811 to form Li_3PO_4. The interface with high electronic conductivity is constructed by attaching graphene fragments to the NCM811 spherical particles. Due to the synergistic effect of the Li_3PO_4 coating layer and the graphene network, the modified sample (GN-LPO-NCM811) exhibits high capacity retention of 94.3% after 150 cycles at 0.5C between 3.0 and 4.3 V, while the pristine material shows a much lower retention of only 88.1%. In addition, the GN-LPO-NCM811 also presents improved cycling stability at elevated temperature of 55 °C. Even at an extremely high rate of 10C, the GN-LPO-NCM811 still remains 70% of its original capacity, while the pristine NCM811 only delivers 50% of the capacity. The stable cycling performance of GN-LPO-NCM811 is demonstrated in a full cell with graphite anode at ambient temperatures. Importantly, the thermal stability of the modified samples is also greatly enhanced. This study provides an effective method to improve the electrochemical performance of $LiNi_{0.8}Co_{0.1}Mn_{0.1}O_2$.

1. Introduction

With the rapid development of electric vehicles (EVs), hybrid electric vehicles (HEVs), and smart devices, those energy storage systems are in great need of high energy density rechargeable batteries [1–3]. Compare to the traditional cathode materials, such as $LiFePO_4$, $LiCoO_2$, and $LiMn_2O_4$, the Ni, Mn, Co based layered oxide cathode materials, especially Ni-rich (Ni content > 0.6), with high specific capacity and low cost, has become the most promising cathode material for next generation lithium-ion batteries [4–7]. However, there are three major problems that prevent its practical application. Firstly, the residual lithium containing species on the surface of Ni-rich NCM absorb the moisture, which bring many troubles to the storage of material and the preparation of cathode slurry [8]; Secondly, the similarity of the ionic

---

[*] Corresponding author.School of Materials and Energy, Guangdong University of Technology, Guangzhou, 510006, PR China.
[**] Corresponding author.

E-mail addresses: zhicong@gdut.edu.cn (Z. Shi), yyang@xmu.edu.cn (Y. Yang).

https://doi.org/10.1016/j.jpowsour.2019.03.014
Received 10 January 2019; Received in revised form 23 February 2019; Accepted 5 March 2019

radius between Li^+ (0.076 nm) and Ni^{2+} (0.069 nm) leads to high interlayer Li/Ni mixing, that facilitates the surface reconstructions of the material during long cycles [9]; Thirdly, the dissolution of transition metal ions not only sacrifice the capacity of cathode, but also deteriorate the full cell performance by depositing transition metals on the anode upon long term cycling [3].

Among all the issues related to the Ni-rich NCM mentioned above, surface residual lithium is the key problem that has to be solved to eliminate its negative effect on manufacturing. In current industrial production, the residual lithium is removed by washing NCM in water followed by a secondary calcination [10]. However, it needs extra energy consumption and may also cause irreversible damage to the surface structure of NCM [11]. Sun et al. creatively transformed the adverse residual lithium species on $LiNi_{0.6}Co_{0.2}Mn_{0.2}O_2$ into favorable Li_3PO_4 coating layer with H_3PO_4 [12]. Wang et al. adopted the analogous method to get rid of the surface residual lithium of $LiNi_{0.8}Co_{0.1}Mn_{0.1}O_2$ via $(NH_4)_2HPO_4$ treatment [13]. Both works showed that coating the Ni-rich NCM with the Li_3PO_4 protective layer result in largely enhanced cycling stability and rate capability. Although the previous reports have shown facile methods for removing the surface residual lithium, and the advantages of Li_3PO_4 coating layer, the relationship between the morphology of Li_3PO_4 coating layer and the conditions of the Li_3PO_4 formation has not been clearly illustrated yet. Meanwhile, the effects of Li_3PO_4 coating layer on cycling properties of NCM at elevated temperature and their thermal stability have not been discussed. Since the Li_3PO_4 coating layer serves as an ion conductor, which only facilitates the Li ion transportation at the electrolyte/electrode interface. Besides, It has reported that a mixed ionic and electronic conductor film constructed with LiF/Cu has greatly improvement on lithium anode [14,15]. We expected that the electrochemical performance of Ni-rich NCM could be further improved by building a mixed ionic and electronic conductor coating layer.

In this work, the residual lithium species of NCM811 ($LiNi_{0.8}Co_{0.1}Mn_{0.1}O_2$) were transformed into Li_3PO_4 coating layer after treating with H_3PO_4 solution (wt.% > 28, before diluted). By controlling the reaction conditions, a Li_3PO_4 coating layer with unique morphology was obtained, which consists of the continuous coating layer and the uniformly distributed nanoparticles. As a super ionic conductor [16], the Li_3PO_4 coating layer not only accelerates the Li^+ diffusion at the interface between active material and electrolyte, but also acts as a barrier to reduce the side reactions. Besides, the tiny particles anchored on the surface preferentially react with the HF in the electrolyte and act as sacrifice to protect the coating layer [13,17]. Thus the continuous coating layer is effectively kept during the cycling lifespan, which produce a stable interface with low impedance.

On the other hand, the intrinsic low electronic conductivity of the Ni-rich NCM material is still a limiting factor for practical application at high current density [5], thus, the electronic conductivity of the material has also been optimized by attaching an proper amount of graphene fragments through a simple physical adsorption method. Benefiting from the mixed-conducting coating layer, the modified sample presents dramatically improved cycling performance at room temperature and high temperature of 55 °C.Owing to the simultaneously optimization of ionic conductivity and electronic conductivity, the GN-LPO-NCM811 half-cell delivers initial capacity of 85 $mAh·g^{-1}$ at 20C when cycled at 55 °C and keeps 80% capacity retention after 400 cycles. Besides the excellent electrochemical performance, the GN-LPO-NCM811 possesses much better thermal stability, which is essential for practical application of Ni-rich cathode material. The systematic research indicated that the design of mixed-conducting layer is an effective method to improve the electrochemical performance of Ni-rich cathode material.

2. Experimental

2.1. Material preparation

2.1.1. Synthesis of $LiNi_{0.8}Co_{0.1}Mn_{0.1}O_2$

All the chemicals for this study were analytical reagents (AR) and were bought from Aladdin Co., Ltd. The $Ni_{0.8}Co_{0.1}Mn_{0.1}(OH)_2$ precursor was purchased from Zhejiang Power New Energy Co., Ltd. The pristine NCM811 ($LiNi_{0.8}Co_{0.1}Mn_{0.1}O_2$) was prepared by mixing $Ni_{0.8}Co_{0.1}Mn_{0.1}(OH)_2$ precursor with $LiOH·H_2O$ at a stoichiometric ratio of 1:1.1. The mixture was calcined at 480 °C for 5 h, followed by sintered at 750 °C for 15 h under flowing oxygen atmosphere.

2.1.2. Synthesis of Li_3PO_4 coating layer

The schematic of the synthesis process is shown in Fig. 1. Typically, 1 wt % H_3PO_4 (0.04 g, wt. $\% \geq 28$, without diluted) was dissolved in 50 mL anhydrous ethanol solution and dispersed by ultrasonic for 10 min. Then the solution was transferred to water bath and 4 g pristine NCM811 were added into the solution. Afterwards, the mixture was stirred at different speed of 300 rpm, 400 rpm and 500 rpm at 80 °C until the solvent was completely evaporated. Finally, the dried powers

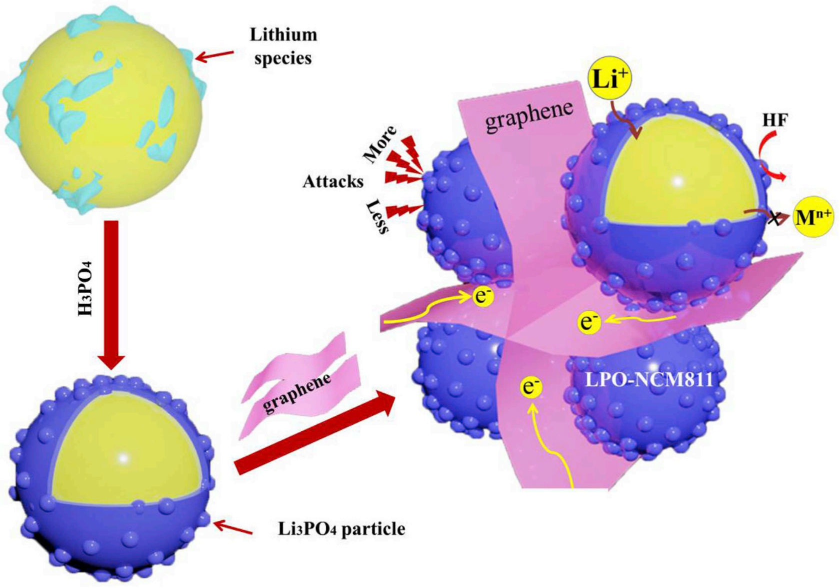

Fig. 1. The synthesis schematic and working mechanism of GN-LPO-NCM811.

were heated in a muffle furnace for 5 h at 500 °C in air. The as-received powder was marked as LPO-NCM811.

2.1.3. Modifying LPO-NCM811 with graphene fragments

The graphene was purchased from Xiamen Kena graphene Technology Co., Ltd. 0.5 wt % or 1 wt % graphene powders were dispersed into 50 mL anhydrous ethanol and treated with ultrasonic at a high frequency of 180 KHz for 2 h. Then 4 g LPO-NCM811 powders were added into the graphene dispersion solution and were stirred at 80 °C until the solvent was completely evaporated. Then the mixture was dried at 120 °C for 10 h under vacuum. Finally, the dried powder was ground thoroughly in an agate mortar. The as-received sample was marked as GN-LPO-NCM811.

2.2. Materials characterization

The crystal information of the prepared materials was analyzed by X-ray diffraction (XRD, Rigaku D/max-2200/PC) with Cu Kα radiation at a scanning rate of 0.02° 2θ/min between 10 and 90°. Time-of-flight (TOF) powder neutron diffraction were measured at the VULCAN instrument at the Spallation Neutron Sources (SNS), Oak Ridge National Laboratory (ORNL) [18]. Approximately 1.6 g of powders were filled into a vanadium sample can with a diameter of 6 mm. The incident neutron beam size was 5 mm × 12 mm, and the diffraction pattern was measured at the detector banks at 2θ = ± 90°, equipped 5 mm receiving collimators. The chopper frequency was selected as 20 Hz, which allows the d-space coverage of 0.45–3.5 Å in the diffracted pattern. Powder neutron diffraction patterns were collected in the high-resolution mode (Δd/d ~0.25%) for a duration of 3 h under the nominal 1.1 MW SNS operation, and then processed using VDRIVE software [19]. Rietveld refinement against the neutron diffraction was performed using General Structure Analysis System (GSAS) software with EXPGUI interface [20,21]. The field-emission scanning electron microscope (FE-SEM, JSM-6700 F, JEOL), transmission electric microscope (TEM, JEOL 2010F), and energy dispersive X-ray spectroscopy (EDS) techniques were performed to confirm the morphology and elemental composition at the surface of the as-prepared materials. The X-ray photoelectron spectroscopy (XPS, ESCAlab250) with Al Kα radiation was used to detect the chemical information on the surface of as-received samples. For DSC measurement, the cells were charged to 4.3 V and kept at 4.3 V for a period of time before disassembled in a glove box. The fully charged active materials were scraped from the electrodes and sealed into the high pressure stainless steel crucible with a small amount of electrolyte. The test was conducted at a heating rate of 5 °C/min between 30 and 400 °C.

2.3. Electrochemical measurement

The electrochemical performance of the prepared materials were tested in the CR2032 coin type cells which were assembled with Li metal as counter electrode in Ar-filled glove box. The cathode electrode was prepared by mixing active material, acetylene black, and polyvinylidene difluoride (PVDF) at a weight ratio of 80:10:10 in N-methylpyrrolidone (NMP). Then the mixed slurry was pasted onto Al current collector. The anode electrode was prepared by mixing graphite, acetylene black and PVDF at a weight ratio of 90:5:5, then the slurry was pasted onto Cu foil. After dried at 120 °C for 12 h under vacuum, both of the electrodes were cut into disks with diameter of 14 mm. The average loading of positive active materials was 4.5 mg cm^{-2}. For the coin-type full cell, the N/P ratio was controlled at 1.1. The electrolyte was 1 M $LiPF_6$ dissolved in EC and DMC (1:1 in volume) solution which contained proper amount of FEC. The assembled cells were aged for 8 h before electrochemical tests. The half cells were firstly charged and discharged at 0.2C (1C = 200 mAh·g^{-1}) for two cycles, then cycled at 0.5C between 3.0 and 4.3 V at 25 or 55 °C. The full cell was firstly activated at 0.1C between 2.8 and 4.2 V for 2 cycles, and then tested at 0.5C for long cycles. All the specific capacities are calculated based on the mass of the pristine NCM811 or the modified composites. The electrochemical impedance spectrum (EIS) was measured at fully charged state after 5 and 30 cycles at a frequency from 100 KHz to 0.005 Hz on an electrochemical working station (Solartron 1287&1260). The CV at different cycles for pristine and modified samples was measured on Zive electrochemical working station.

3. Results and discussions

Fig. 2 shows the surface morphology of pristine and modified samples. Fig. 2 (e) clearly shows the uniformly distributed tiny particles on the surface of LPO-NCM811, while the pristine NCM811 displays smooth surface. It's noticeable that the different surface morphologies can be simply obtained by changing the stirring speed during the Li_3PO_4 treatment (Fig. S1). When the stirring speed was too low, nanosheet-like Li_3PO_4 was obtained. With the increase of stirring speed, rod-like and granular Li_3PO_4 was formed on the surface of active material. When the mixture was stirred at suitable speed, the rough surface consisting of continuous coating layer and randomly distributed particles was obtained. The electrochemical properties of LPO-NCM811s with different morphologies are shown in Fig. S2 (Supporting information). The LPO-NCM811 formed at 500r/min presents the best cycling stability. The SEM images of GN-LPO-NCM811 in Fig. 2 (c, f) indicate that the graphene fragments are successfully attached on the surface of the material after a simple adsorption process. The EDS

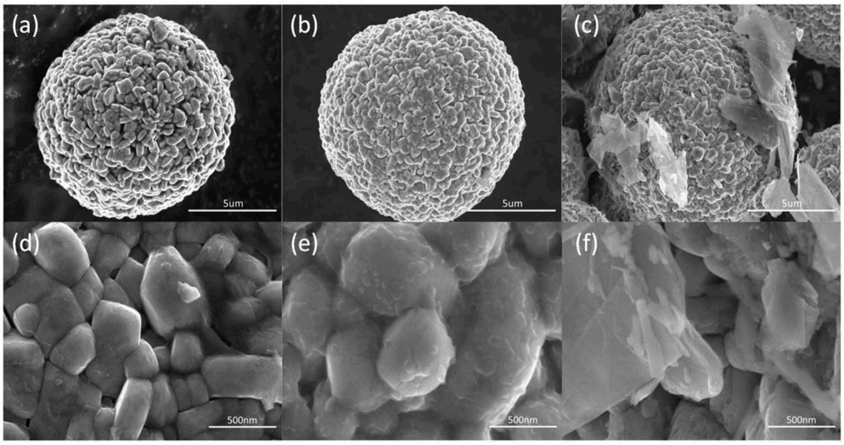

Fig. 2. The SEM images of pristine NCM811 (a, d), LPO-NCM811 (b, e), and GN-LPO-NCM811 (c, f).

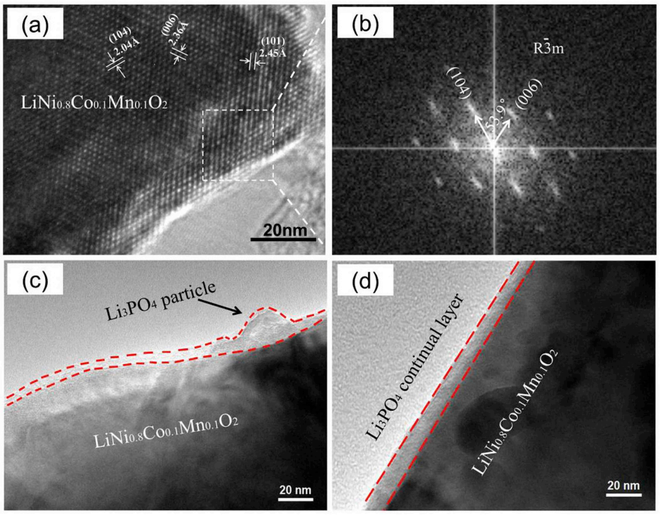

Fig. 3. TEM images of pristine NCM811 (a) and the corresponding FFT patterns (b) taken from the selected region in (a). TEM images of the Li_3PO_4 particle (c) and the continual Li_3PO_4 coating layer (d) on the surface of LPO-NCM811.

mapping of the Ni, Co, Mn, C and P elements for GN-LPO-NCM811 are shown in Fig. S3 (Supporting information). The density of P element was relatively high in some area, which corresponds to the Li_3PO_4 particles on top of the Li_3PO_4 surface layer. The C element belongs to graphene are also observed in Fig. S3 (Supporting information).

The TEM was performed to further investigate the morphology at the surface of LPO-NCM811. The well-ordered lattice fringes were observed in Fig. 3 (a), indicated the pristine NCM811 is highly crystallized. The corresponding fast Fourier transform (FFT) pattern of the selected square in Fig. 3a confirms the layered structured of pristine NCM811 [22]. The amorphous Li_3PO_4 coating layer was observed in Fig. 3 (c) and 3 (d). Here the Li_3PO_4 coating layer consists of two different configurations, one is the uniform continuous coating layer with a thickness of 10 nm (Fig. 3 (d)), and the other one is the nanosized particles anchored on top of the Li_3PO_4 coating layer (Fig. 3 (c)). This unique coating layer in our work is quite different from the previous reports, because the reported Li_3PO_4 coating layers comprise either the continuous layer or the single distributed particles [12,13,16]. The observed morphology by TEM is highly consistent with the SEM images in Fig. 2 (e).

The crystal phases of pristine and modified samples were confirmed by powder X-ray diffraction technique. The results of Rietveld refinement of XRD for pristine NCM811, LPO-NCM811 and GN-LPO-NCM811 are shown in Fig. S4 (Supporting information). It indicates that all samples have hexagonal α-$NaFeO_2$ structure belongs to the *R*3*m* space group [23–25]. No obvious changes were observed in XRD peaks after surface modifications, suggesting that the layered phase is well maintained. It is notable that Li_3PO_4 phase were not detected from the XRD patterns, which may be attributed to the low content or the amorphous phase caused by the low calcination temperature and short calcination time. However, the trace graphene was detected even though the content is only 0.5 wt %. Table S1 (Supporting information) shows the lattice parameters based on the refined results of XRD data of pristine and modified samples. The c lattice parameter of modified samples was slightly decreased compared to the pristine NCM811. This may associate with the further calcination after removing the residual lithum species with H_3PO_4 solution, which leads to the slightly increase of Ni^{2+} in Li layers [26].

The neutron diffraction, which possesses the advantages of sensing light elements and revealing structure ordering [27,28], was employed to quantify the degree of Li/Ni mixing in these materials [29]. The neutron diffraction patterns along with Rietveld refinement of pristine NCM811 and LPO-NCM811 are shown in Fig. 4. The results show that the Li/Ni mixing degree for LPO-NCM811 was slightly higher than the pristine one. This change might be attributed to the secondary calcination process during the formation of the amorphous phase Li_3PO_4. This result is in good agreement with the literature [26] and XRD results.

The XPS was conducted to illustrate the changes of the surface chemical species of pristine and modified samples (Fig. 5). The binding energy (BE) of P 2p at 133.1 eV is observed for GN-LPO-NCM811, which corresponds to the [PO4] group in coating layer [30]. The C 1s spectra of the pristine NCM811 and GN-LPO-NCM811 are quite different. The peak at 289.3 eV corresponds to the MCO_3 caused by the residual lithium carbonates at the surface of pristine NCM811 [31]. This peak is not detected in the modified samples, which strongly confirms that the residual lithium species are successfully removed by H_3PO_4 modification. Besides, the peaks at O-C = O (289.6 eV) and C-C (285 eV) in GN-LPO-NCM811 are assigned to the graphene fragments on the surface of GN-LPO-NCM811 [32,33]. The peak position of O 1s has a slight shift, which indicates the chemical environment of O has changed. The Ni 2p, Co $2p_{3/2}$, and Mn $2p_{3/2}$ peaks of pristine and modified samples are almost identical [34,35], indicating that this composite modification does not change the chemical environments of transition elements (M^{n+}) at the surface of NCM811.

The effects of the mixed-conducting coating layer on electrochemical performance of NCM811 were systematically studied. The initial charge and discharge profiles of pristine and modified samples are shown in Fig. 6, and the initial discharge capacity and coulomb efficiency for all the samples cycled at 25 °C and 55 °C are shown in Table 1. They were cycled at 25 °C between 3.0 and 4.3 V at 0.2C ($1C = 200\ mAh{\cdot}g^{-1}$). The initial coulombic efficiency for LPO-NCM811 and GN-LPO-NCM811 were enhanced to 81.2% and 82.7% from 76.9%, respectively. Though the initial coulombic efficiencies and charge/discharge capacities for all the samples were much higher at high

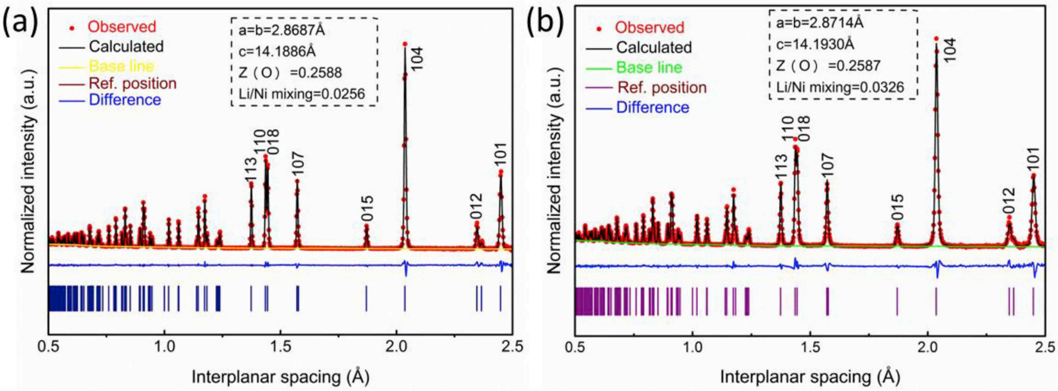

Fig. 4. The Neutron diffraction results for pristine NCM811 (a) and LPO-NCM811 (b).

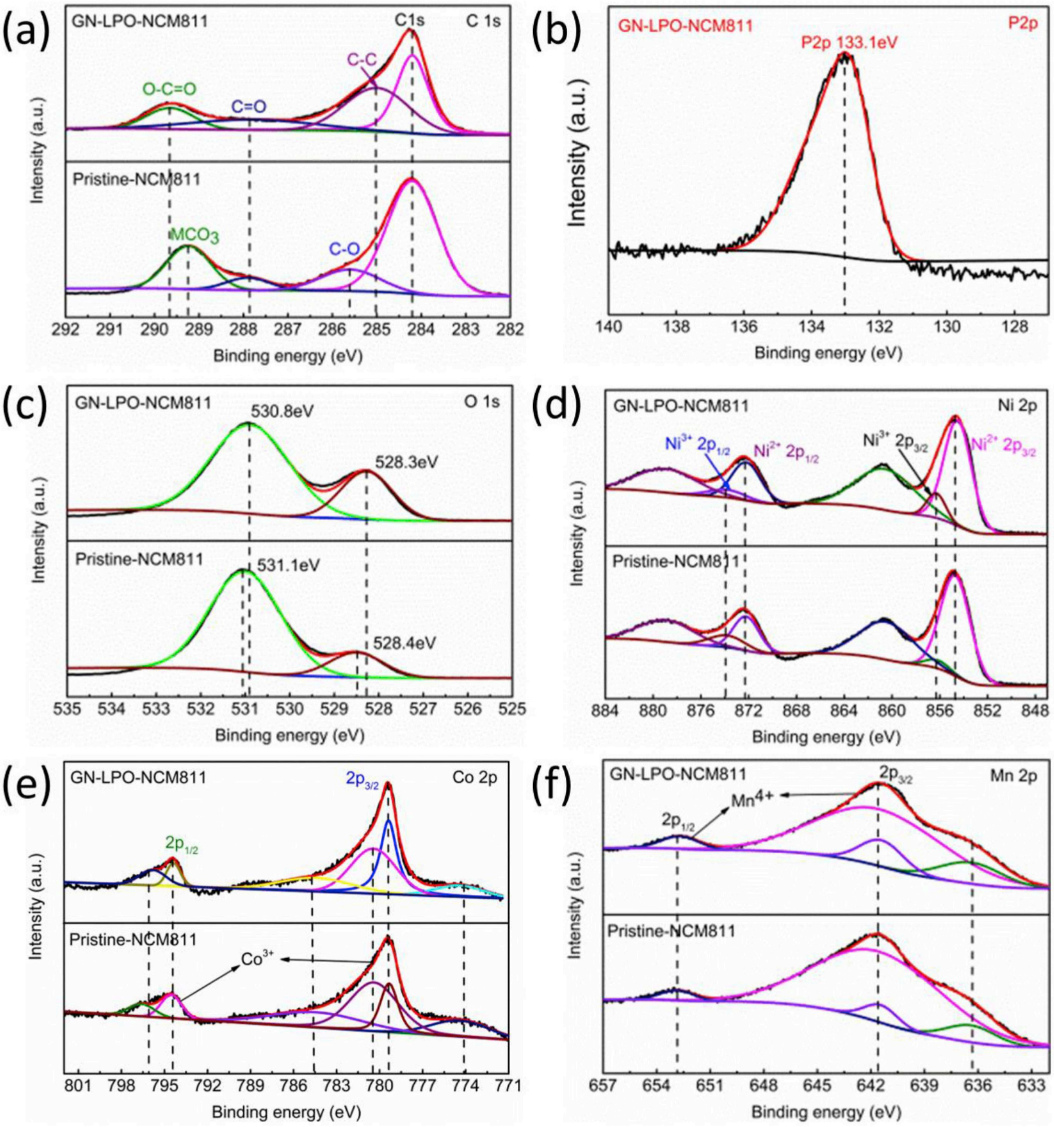

Fig. 5. XPS results for C 1s, P 2p, O 1s, Ni 2p, Co 2p and Mn 2p of pristine NCM811 and GN-LPO-NCM811.

temperature than at room temperature [36], the enhanced initial coulombic efficiency for modified samples were still evident when the cells were cycled at 55 °C. This is due to the protective Li_3PO_4 layer, which effectively reduces the side reactions at the electrolyte and material interface. According to the previous reports [37,38], the side reactions are highly associated with the capacity degradation during long cycling lifespan. Consequently, the Li_3PO_4 coating layer is expected to enhance the cycling stability of NCM811. The cycling performance was tested at 0.5C between 3.0 and 4.3 V, LPO-NCM811 and GN-LPO-NCM811 showed capacity retentions of 93.5% and 94.3% after 150 cycles, which is much higher than 88.1% for pristine NCM811. The improvement became more significant when the samples were cycled at high temperature of 55 °C. The LPO-NCM811 and GN-LPO-NCM811 retained 92.1% and 94.2% of their initial capacities after 100 cycles, while the pristine NCM811 showed low capacity retention of 75.5%. Fig. 6e shows the excellent cycling stability of GN-LPO-NCM811/graphite coin-type full cell over the course of 700 cycles. The cell was cycled between 2.8 and 4.2 V at 0.5C, it maintained 80% of its capacity after 700 cycles. Their charge/discharge voltage profiles are presented in Fig. S5.

In order to evaluate the rate capability of the modified samples, all the samples were measured at various current density of 0.2, 0.5, 1, 2, 5, and 10C between 3.0 and 4.3 V (Fig. 7). Both of the modified NCM811 showed better rate capacity than the pristine NCM811. The improvements on their rate capabilities are attributed to two aspects: firstly, the Li_3PO_4 coating layer possess fast ionic conductivity [39], which accelerates Li^+ diffusion at the interface of the material; secondly, the existence of graphene fragments further reduce the reaction kinetics of cathode materials by increasing the electronic conductivity of the modified sample [5,40]. Due to the synergetic effects of Li_3PO_4 and graphene, the GN-LPO-NCM811 exhibits notable capacity retention at high current density. At the high rate of 10C, the GN-LPO-NCM811 delivers 70% (122.4 $mAh·g^{-1}$) of its initial capacity. As a comparison, the pristine NCM811 shows only 50% (108.5 $mAh·g^{-1}$) capacity at 10C, the.

LPO-NCM811 sits between pristine NCM811 and GN-LPO-NCM811. The influence of graphene content on the rate capabilities was also compared in Fig. S7 (Supporting information). The high rate capability of GN-LPO-NCM811 was tested at an extremely high rate of 20C (3 min per charge or discharge). The cell delivered initial discharge capacity of 85 $mAh·g^{-1}$, and remained 80% capacity after 400 cycles (Fig. 7 (e)).

The electrochemical impedance spectroscopy technique was conducted on the three samples at fully charged state after 5 and 30 cycles to reveal the reasons for the enhanced rate capacity. The cells were cycled at 0.5C between 3.0 and 4.3 V. The fitting results and equivalent

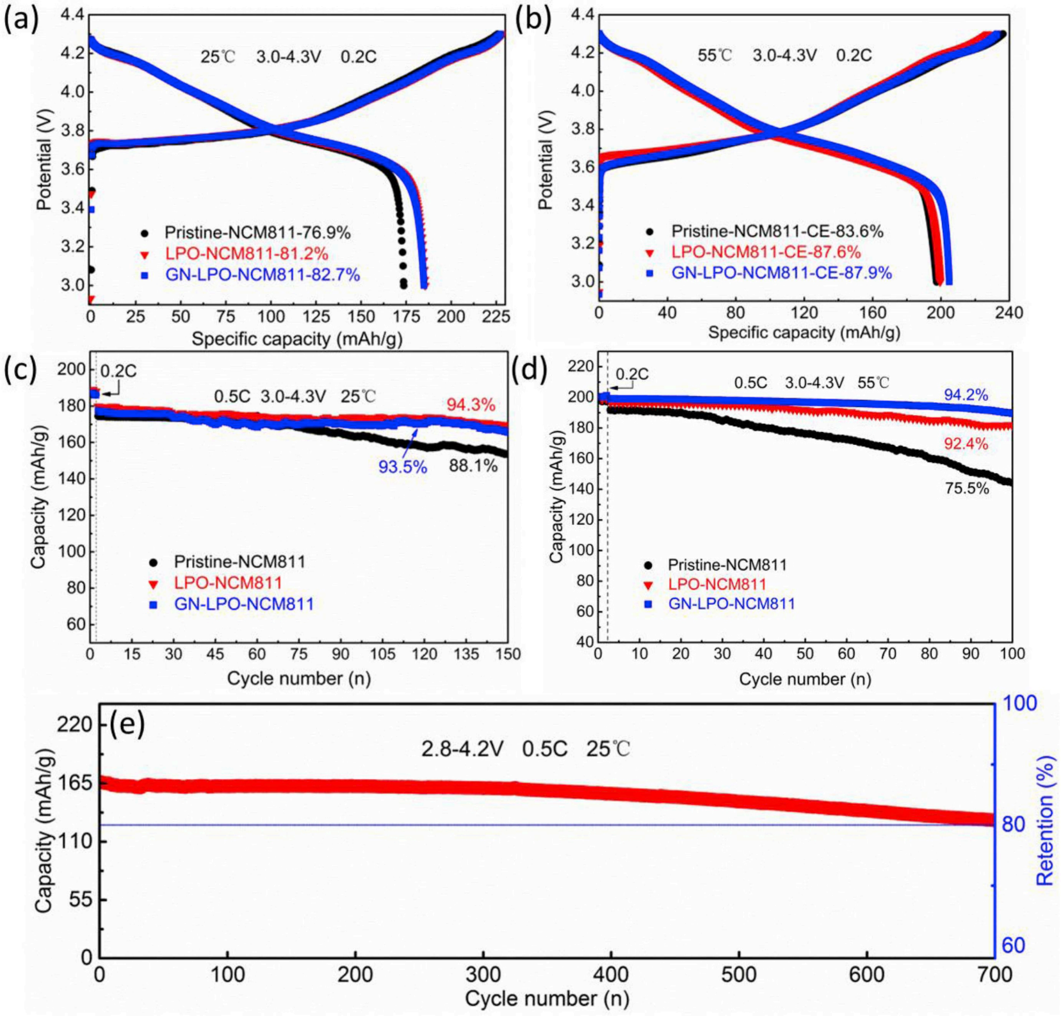

Fig. 6. The initial charge and discharge curves for pristine and modified samples at 25 °C (a) and 55 °C (b), the cycling performance for pristine and modified samples in the voltage range 3.0–4.3 V at 0.5 C at 25 °C (c) and 55 °C (d), and the cycling performance of the full-cell for GN-LPO-NCM811 in the voltage range 2.8–4.2 V at 0.5 C at 25 °C.

Table 1
The initial discharge capacity and coulomb efficiency for all the samples cycled at 25 °C and 55 °C.

	Discharge capacity (mAh·g^{-1})		Initial coulomb efficiency	
	25 °C	55 °C	25 °C	55 °C
pristine NCM811	173.7	197.4	76.9%	83.6%
LPO-NCM811	185.6	199.4	81.2%	87.6%
GN-LPO-NCM811	184.9	204.8	82.7%	87.9%

circuits of the EIS are shown in Fig. 8 (a, b). The semicircle at high frequency region stands for the solid electrolyte impedance (SEI), the semicircle at middle frequency region represents the charge transfer impedance, and the sloped line at low frequency corresponds to the Warburg impedance which represents the Li$^+$ diffusion in bulk phase [41]. Table 2 shows the fitting results of R_f and R_{ct} of pristine and modified samples. The R_f values of LPO-NCM811 and GN-LPO-NCM811 slightly increased from 5th cycle to 30th cycle. The R_{ct} of the three samples show significant difference after 30 cycles. Though the Rct values of three samples get increased, the GN-LPO-NCM811 shows the lowest increment. This is benefit from the simultaneously improved ionic and electronic conductivities by the Li_3PO_4 coating layer and graphene fragments.

The EIS technique was also used to calculate the Li$^+$ diffusion in bulk phase [42,43]. The slopy line at low frequency region is associated with the Li$^+$ diffusion in electrode. According to the formula below (1) [42–44]:

The values of gas constant (R), absolute temperature (T) and Faraday constant (F) are known. n is the number of charge transfer, A represents the active electrode area, The $C_{Li}{}^+$ can be calculated based on the unit volume in Table S1 (Supporting information). The Warburg factor (σ) can be calculated according to formula (2) below and the fitting results in Fig. 8 (c).

$$Z' = R_s + R_{ct} + \sigma\omega^{-1/2} \tag{2}$$

The calculated values of diffusion coefficient of Li$^+$ ($D_{Li}{}^+$) for pristine NCM811, LPO-NCM811, and GN-LPO-NCM811 are $8.57 \times 10^{-13}\ cm^2\ s^{-1}$, $1.19 \times 10^{-12}\ cm^2\ s^{-1}$ and $2.31 \times 10^{-12}\ cm^2\ s^{-1}$, respectively. The results indicate that this synergistic mixed-conducting coating layer successfully improved the Li$^+$ diffusion coefficient of the materials. The enhanced properties are attributed to the high ionic conductivity of Li_3PO_4 and the excellent electronic conductivity of graphene.

According to previous literature, $LiPF_6$ will break down when the electrolyte contains a trace amount of H_2O and generate HF [45]. HF can react with the residual lithium species (LiOH or Li_2CO_3) and

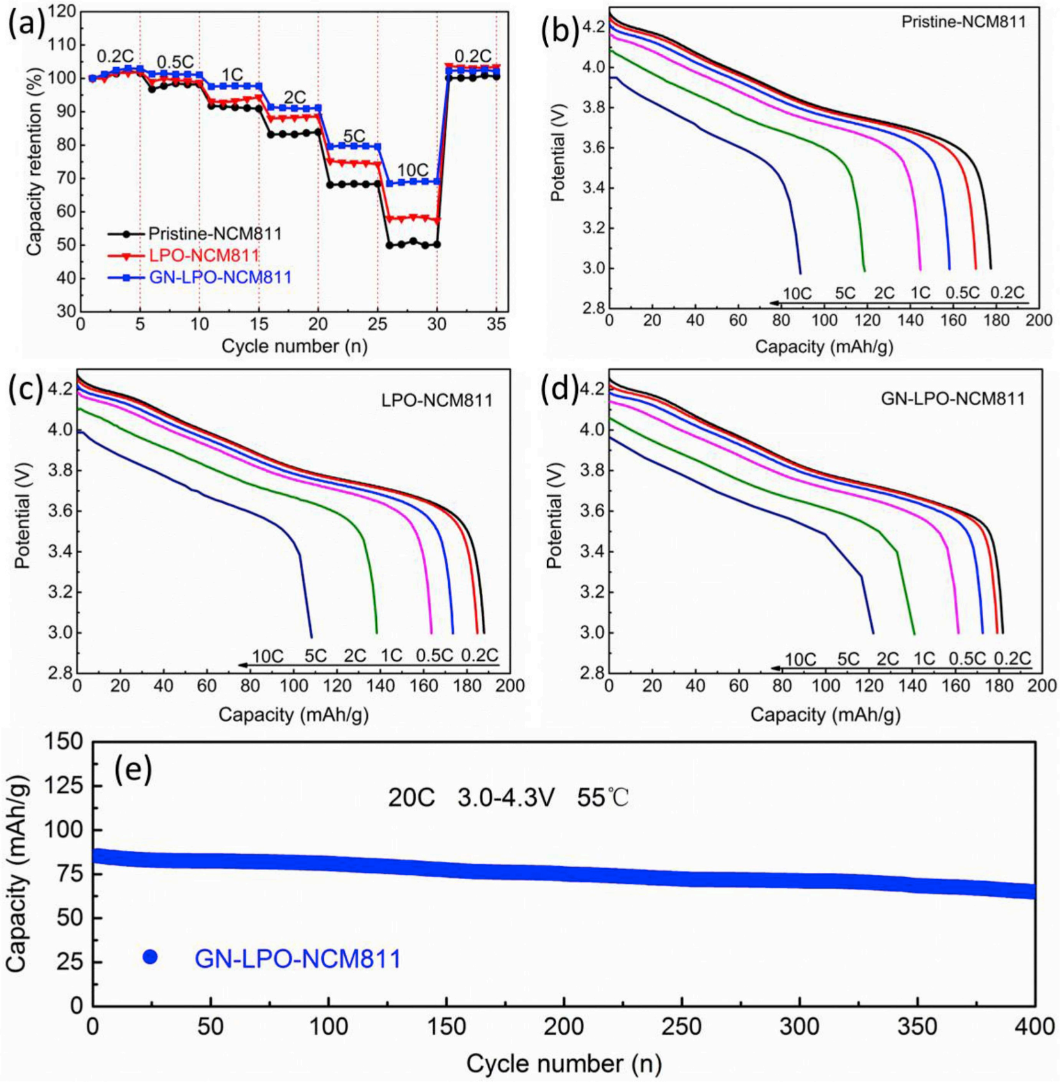

Fig. 7. The relative capacity retentions for pristine and modified samples at different current density (a). The discharge curves at different rates for pristine NCM811 (b), LPO-NCM811(c), and GN-LPO-NCM811 (d). The cycling performance of the half-cell for GN-LPO-NCM811 in the voltage range 3.0–4.3 V at rate of 20 C at 55 °C.

produce H_2O again [46,47]. In our research, the residual lithium species were removed after treating with H_3PO_4 solution and transformed into Li_3PO_4 coating layer. This transformation can effectively mitigate HF related side reactions mentioned above. Meanwhile, Li_3PO_4 can also directly react with HF without producing H_2O [12]. Therefore, the transformation of residual lithium species to Li_3PO_4 directly restrains the generation of HF in electrolyte. As a consequence, the cycling stability is greatly enhanced at both room temperature and elevated temperature. The previous researches also reported that small amount of tiny particles such as TiO_2 [17], Li_3PO_4 [16] etc. anchored on the surface of the material also improve the electrochemical properties greatly, which suggest that these particles are preferentially involved in the side reactions. The working mechanism of the mixed-conducting coating layer in this study is described in Fig. 1. The Li_3PO_4 coating layer, which consists of the continuous coating layer and tiny particles on top of it provide protection against HF attack. As long as the side reactions preferentially happened with the exposed Li_3PO_4 particles, the damages to the continuous coating layer are effectively alleviated. This contributes to a stable interface which is confirmed by the EIS results. Meanwhile, the previous reports has reported that the Li_3PO_4 coating layer could effectively reduce the dissolution of transition mental ions of Ni-rich cathode material [48,49], thus the original structure of material can be well maintained in long cycling. On the other hand, the introduction of graphene build electron conducting network between NCM811 spherical particles, which further accelerates the transportation of electrons. Finally, the GN-LPO-NCM811 possesses the merits of fast ionic transportation and high electronic transfer at the same time.

The thermal stability of NCM cathode material at charged state is the key issue in judging the safety of lithium battery in practical applications [1,40]. The DSC results for Pristine and modified samples at the charged state of 4.3 V are shown in Fig. 8 (d). The main exothermic peak for pristine NCM811 was located at 241.9 °C with the high reaction heat of 1274 J. The main exothermic peaks for LPO-NCM811 and GN-LPO-NCM811 were shifted to 246.9 °C and 256.5 °C, respectively. In addition, the reaction heat for two modified samples were remarkably decreased to 1064 J and 1032 J. This changes manifest that the coating layer prevents the direct contact between the highly unstable NCM811 surface and electrolyte [36], therefore, the reactivity at the interface is effectively reduced. More importantly, the coating layer can inhibit oxygen release from the bulk phase and then raise the occurrence temperature of exothermic reactions and lower the reaction heat. Interestingly, although the amount of graphene fragments induced is only 0.5 wt %, its influence on the thermal stability of the material is non-negligible.

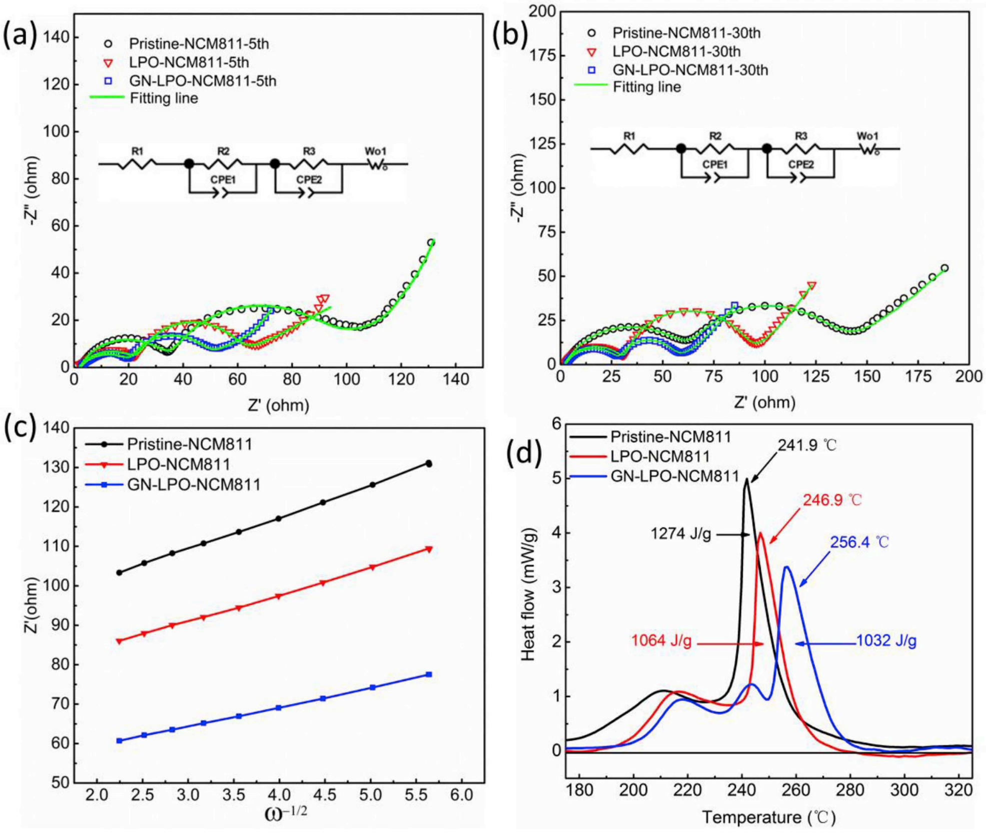

Fig. 8. The fitting results of EIS at charged state after 5 (a) and 30 (b) cycles at 0.5C. The relationships between Z real and $\omega^{-1/2}$ at low frequency based on the EIS results before cycling (c). The differential scanning calorimetry traces showing heat flow from the reaction of the electrolyte with pristine NCM811, LPO-NCM811, and GN-LPO-NCM811 charged to 4.3 V (d).

$$D_{Li^+} = \frac{R^2T^2}{2n^4F^4A^2C_{Li^+}^2\sigma^2} \tag{1}$$

Table 2
The fitting results of R_f and R_{ct}, and the calculated D_{Li^+} from electrochemical impedance spectra of pristine NCM811, LPO-NCM811, GN-LPO-NCM811 electrodes after 5 and 30 charge-discharge cycles.

	pristine NCM811		LPO-NCM811		GN-LPO-NCM811	
	R_f	R_{ct}	R_f	R_{ct}	R_f	R_{ct}
5th	34.3	102.1	21.9	64.9	19.5	51.6
30th	61.6	142.3	30.5	95.9	28.1	59.3
D_{Li^+}	$8.57 \times 10^{-13}\,cm^2\,s^{-1}$		$1.19 \times 10^{-12}\,cm^2\,s^{-1}$		$2.31 \times 10^{-12}\,cm^2\,s^{-1}$	

4. Conclusion

In summary, a unique synergistic multifunctional coating layer was constructed on the surface of $LiNi_{0.8}Co_{0.1}Mn_{0.1}O_2$ by transforming the residual lithium species into Li_3PO_4 and attaching graphene fragments. Microscopy studies revealed that a 10 nm amorphous Li_3PO_4 layer along with nanosized Li_3PO_4 particles uniformly cover the surface of NCM811, the graphene fragments connect NCM spherical particles to form electronic network. The XPS and neutron diffraction results confirmed that the surface modifications remove the lithium containing residuals and form coating layers without changing the crystal structure and surface transition metal chemistries of NMC811. As a result, the GN-LPO-NCM811 exhibits outstanding electrochemical performance, it delivers 70% of its initial capacity at an extremely high rate of 10C. Its excellent cycling stability is demonstrated in a coin-type full cell, it maintains 80% of its original capacity after 700 cycles at 0.5C. At elevated temperature of 55 °C, the half-cell of GN-LPO-NCM811 achieves a high capacity retention of 80% after 400 cycles at 20C. As evidenced from the EIS studies, the Li_3PO_4 not only protects the materials from side reactions with the electrolytes, but also facilitates the Li^+ transportation at the electrode/electrolyte interface. At the same time, the electronic network bridged by graphene fragments offers fast electron transfer. Due to the protection from the mixed-conducting coating layer, the thermal stability is significantly improved as well. This study clearly demonstrates that an effective surface modification should possess both high ionic conductivity and excellent electronic conductivity. These insights will provide guidance for engineering the surface of Ni-rich NCM cathode materials of the future.

This manuscript has been authored by UT-Battelle, LLC under Contract No. DE-AC05-00OR22725 with the U.S. Department of Energy. The United States Government retains and the publisher, by accepting the article for publication, acknowledges that the United States Government retains a non-exclusive, paid-up, irrevocable, worldwide license to publish or reproduce the published form of this manuscript, or allow others to do so, for United States Government purposes. The Department of Energy will provide public access to these results of federally sponsored research in accordance with the DOE Public Access Plan (http://energy.gov/downloads/doe-public-access-plan).

Acknowledgement

This work was supported by the National Natural Science Foundation, China (Nos. 21673051 and 51604086), the Department of Science and Technology of Guangdong Province, China (No. 2017B010119003), the “One-hundred Talents plan” (No. 220418056), and the Youth Foundation of Guangdong University of Technology, China (No. 252151038). Neutron diffraction work was carried out at the Spallation Neutron Source (SNS), which is the U.S. Department of Energy (DOE) user facility at the Oak Ridge National Laboratory, sponsored by the Scientific User Facilities Division, Office of Basic Energy Sciences. The authors thank Mr. M. J. Frost at SNS for the technique support.

Appendix A. Supplementary data

Supplementary data to this article can be found online at https://doi.org/10.1016/j.jpowsour.2019.03.014.

References

[1] Y.K. Sun, S.T. Myung, B.C. Park, J. Prakash, I. Belharouak, K. Amine, Nat. Mater. 8 (2009) 320–324.
[2] B. Scrosati, J. Garche, J. Power Sources 195 (2010) 2419–2430.
[3] W. Liu, P. Oh, X. Liu, M.J. Lee, W. Cho, S. Chae, Y. Kim, J. Cho, Angew Chem. Int. Ed. Engl. 54 (2015) 4440–4457.
[4] W.Y. Yujing Bi, Rui Du, Jingjing Zhou, Meng Liu, Yang Liu, Deyu Wang, J. Power Sources 283 (2015) 211–218.
[5] S.S. Jan, S. Nurgul, X. Shi, H. Xia, H. Pang, Electrochim. Acta 149 (2014) 86–93.
[6] S.-H. Lee, C.S. Yoon, K. Amine, Y.-K. Sun, J. Power Sources 234 (2013) 201–207.
[7] M.D. Radin, S. Hy, M. Sina, C. Fang, H. Liu, J. Vinckeviciute, M. Zhang, M.S. Whittingham, Y.S. Meng, A. Van der Ven, Adv. Energy Materials 7 (2017) 1602888.
[8] Y. Ding, B.W. Deng, H. Wang, X. Li, T. Chen, X.X. Yan, Q. Wan, M.Z. Qu, G.C. Peng, J. Alloy. Comp. 774 (2019) 451–460.
[9] Y. Cho, P. Oh, J. Cho, Nano Lett. 13 (2013) 1145–1152.
[10] G.K. Min, J. Kim, Y. Hong, K.S. Ryu, J. Cho, Electrochem. Solid State Lett. 9 (2014) A19–A23.
[11] R. Moshtev, P. Zlatilova, S. Vasilev, I. Bakalova, A. Kozawa, J. Power Sources 81–82 (1999) 434–441.
[12] C.-H. Jo, D.-H. Cho, H.-J. Noh, H. Yashiro, Y.-K. Sun, S.T. Myung, Nano Research 8 (2014) 1464–1479.
[13] X. Xiong, D. Ding, Y. Bu, Z. Wang, B. Huang, H. Guo, X. Li, J. Mater. Chem. 2 (2014) 11691–11696.
[14] C. Yan, X.B. Cheng, Y.X. Yao, X. Shen, B.Q. Li, W.J. Li, R. Zhang, J.Q. Huang, H. Li, Q. Zhang, Adv. Mater. 30 (2018) e1804461.
[15] X.-B. Cheng, C. Yan, X.-Q. Zhang, H. Liu, Q. Zhang, ACS Energy Letters 3 (2018) 1564–1570.
[16] H.G. Song, J.Y. Kim, K.T. Kim, Y.J. Park, J. Power Sources 196 (2011) 6847–6855.
[17] X. Yuan, Q.-j. Xu, X. Liu, H. Liu, Y. Min, Y. Xia, Electrochim. Acta 213 (2016) 648–654.
[18] K. An, H.D. Skorpenske, A.D. Stoica, D. Ma, X.L. Wang, E. Cakmak, Metall. Mater. Trans. 42A (2011) 95–99.
[19] K. An, X.L. Wang, A.D. Stoica, ORNL Report, ORNL-TM-2012-621, Oak Ridge National Laboratory, 2012.
[20] A.C. Larson, R.B.V. Dreele, Los Alamos National Laboratory Report, LAUR, 2004, pp. 86–748.
[21] B.H. Toby, J. Appl. Crystallogr. 34 (2001) 210–213.
[22] B. Han, S. Xu, S. Zhao, G. Lin, Y. Feng, L. Chen, D.G. Ivey, P. Wang, W. Wei, ACS Appl. Mater. Interfaces 10 (2018) 39599–39607.
[23] G. Li, Z. Zhang, R. Wang, Z. Huang, Z. Zuo, H. Zhou, Electrochim. Acta 212 (2016) 399–407.
[24] H. Liu, H. Liu, I.D. Seymour, N. Chernova, K.M. Wiaderek, N.M. Trease, S. Hy, Y. Chen, K. An, M. Zhang, O.J. Borkiewicz, S.H. Lapidus, B. Qiu, Y. Xia, Z. Liu, P.J. Chupas, K.W. Chapman, M.S. Whittingham, C.P. Grey, Y.S. Meng, J. Mater. Chem. 6 (2018) 4189–4198.
[25] H. Liu, H. Liu, Saul H. Lapidus, Y. Shirley Meng, Peter J. Chupas, Karena W. Chapman, J. Electrochem. Soc. 164 (9) (2017) A1802–A1811.
[26] J.H. Jo, C.-H. Jo, H. Yashiro, S.-J. Kim, S.-T. Myung, J. Power Sources 313 (2016) 1–8.
[27] Y. Chen, Y. Cheng, J. Li, M. Feygenson, W.T. Heller, C. Liang, K. An, Adv. Energy Materials 7 (2017) 1601950.
[28] Y. Chen, E. Rangasamy, C. Liang, K. An, Chem. Mater. 27 (2015) 5491–5494.
[29] H. Liu, Y. Chen, S. Hy, K. An, S. Venkatachalam, D. Qian, M. Zhang, Y.S. Meng, Adv. Energy Materials 6 (2016) 1502143.
[30] K. Tan, M. Reddy, G. Rao, B. Chowdari, J. Power Sources 141 (2005) 129–142.
[31] P. Yue, Z.X. Wang, H.J. Guo, X.H. Xiong, X.H. Li, Electrochim. Acta 92 (2013) 1–8.
[32] C. Chen, Y. He, G. Xiao, Y. Xia, H. Li, Z. He, Appl. Surf. Sci. 444 (2018) 511–521.
[33] X. Li, X. Xu, F. Xia, L. Bu, H. Qiu, M. Chen, L. Zhang, J. Gao, Electrochim. Acta 130 (2014) 305–313.
[34] Z. Chen, D. Chao, J. Lin, Z. Shen, Mater. Res. Bull. 96 (2017) 491–502.
[35] Y. Ding, R. Wang, L. Wang, K. Cheng, Z. Zhao, D. Mu, B. Wu, Energy Procedia 105 (2017) 2941–2952.
[36] Y.S. Lee, W.K. Shin, A.G. Kannan, S.M. Koo, D.W. Kim, ACS Appl. Mater. Interfaces 7 (2015) 13944–13951.
[37] Z. Chen, D. Chao, J. Lin, Z. Shen, Mater. Res. Bull. 96 (2017) 491–502.
[38] Y. Ding, R. Wang, L. Wang, K. Cheng, Z. Zhao, D. Mu, B. Wu, Energy Procedia 105 (2017) 2941–2952.
[39] S. Chen, T. He, Y. Su, Y. Lu, L. Bao, L. Chen, Q. Zhang, J. Wang, R. Chen, F. Wu, ACS Appl. Mater. Interfaces 9 (2017) 29732–29743.
[40] J.H. Shim, Y.M. Kim, M. Park, J. Kim, S. Lee, ACS Appl. Mater. Interfaces 9 (2017) 18720–18729.
[41] X. Wang, H. Hao, J. Liu, T. Huang, A. Yu, Electrochim. Acta 56 (2011) 4065–4069.
[42] M. Wang, M. Luo, Y. Chen, Y. Su, L. Chen, R. Zhang, J. Alloy. Comp. 696 (2017) 907–913.
[43] F. Wu, X. Zhang, T. Zhao, L. Li, M. Xie, R. Chen, J. Mater. Chem. 3 (2015) 9528–9537.
[44] X. Wang, H. Hao, J. Liu, T. Huang, A. Yu, Electrochim. Acta 56 (2011) 4065–4069.
[45] K. Edström, T. Gustafsson, J.O. Thomas, Electrochim. Acta 50 (2004) 397–403.
[46] Y. Bi, T. Wang, M. Liu, R. Du, W. Yang, Z. Liu, Z. Peng, Y. Liu, D. Wang, X. Sun, RSC Adv. 6 (2016) 19233–19237.
[47] M.-J. Lee, M. Noh, M.-H. Park, M. Jo, H. Kim, H. Nam, J. Cho, J. Mater. Chem. 3 (2015) 13453–13460.
[48] H. Ci, H. Ren, Y. Qi, X. Chen, Z. Chen, J. Zhang, Y. Zhang, Z. Liu, Nano Research 11 (2018) 3106–3115.
[49] J. Zhu, Y. Li, L. Xue, Y. Chen, T. Lei, S. Deng, G. Cao, J. Alloy. Comp. 773 (2019) 112–120.